# *Daytime CO2 urban surface fluxes from airborne measurements, eddy-covariance observations and emissions inventory in Greater London*

Article

Accepted Version

Font, A., Grimmond, C. S. B., Kotthaus, S., Morguí, J. -A., Stockdale, C., O'Connor, E., Priestman, M. and Barratt, B. (2015) Daytime CO2 urban surface fluxes from airborne measurements, eddy-covariance observations and emissions inventory in Greater London. Environmental Pollution, 196. pp. 98-106. ISSN 0269-7491 doi: https://doi.org/10.1016/j.envpol.2014.10.001 Available at http://centaur.reading.ac.uk/37905/

Published version at: http://dx.doi.org/10.1016/j.envpol.2014.10.001
To link to this article DOI: http://dx.doi.org/10.1016/j.envpol.2014.10.001

Publisher: Elsevier

# Daytime $CO_2$ urban surface fluxes from airborne measurements, eddy-covariance observations and emissions inventory in Greater London

A. Font[1], C. S. B. Grimmond[2], S. Kotthaus[2,4], J.-A. Morguí[3], C. Stockdale[2], E. O'Connor[2], M. Priestman[1] and B. Barratt[1]

1 MRC HPA Centre for Environment and Health, King's College London, 150 Stamford Street, SE1 9NH, London, UK

2 Department of Meteorology, University of Reading, Earley Gate, PO Box 243, Reading, RG6 6BB, UK

3 Institut Català de Ciències del Clima, Dr. Trueta 203, 08005, Barcelona, Spain

4 King's College London, Department of Geography, The Strand, WC2R 2LS, London, UK

Corresponding author: A. Font (anna.font_font@kcl.ac.uk, telephone: +44 2078484018, fax: +44 2078484045)

## Abstract

Airborne measurements within the urban mixing layer (360 m) over Greater London are used to quantify $CO_2$ emissions at the meso-scale. Daytime $CO_2$ fluxes, calculated by the Integrative Mass Boundary Layer (IMBL) method, ranged from 46 to 104 µmol $CO_2$ $m^{-2}$ $s^{-1}$ for four days in October 2011. The day-to-day variability of IMBL fluxes is at the same order of magnitude as for surface eddy-covariance fluxes observed in central London. Compared to fluxes derived from emissions inventory, the IMBL method gives both lower (by -37%) and higher (by 19%) estimates. The sources of uncertainty of applying the IMBL method in urban areas are discussed and guidance for future studies is given.

**Capsule**: $CO_2$ airborne-derived fluxes by Boundary Layer Mass balance are an independent measure of meso-scale urban fluxes complementing urban eddy-covariance fluxes and emissions inventory

**Key words**: carbon dioxide; urban fluxes; aircraft surveys; eddy covariance; megacity, emissions inventory

## 1 Introduction

Urban areas are responsible for 70% of greenhouse gas (GHG) emissions despite covering only 2% of the world's surface (IEA 2008). Knowledge of both concentrations and fluxes are needed to understand how urban emissions affect regional carbon exchanges (Duren and Miller 2012).

Measurements of urban atmospheric $CO_2$ concentrations are becoming a common means to study local GHG emissions and urban carbon cycles (Velasco and Roth 2010; Christen 2014). An enhancement of the $CO_2$ concentration of the urban canopy layer (UCL) is consistently observed in cities (e.g. Idso et al. 1998). However, urban $CO_2$ concentrations can show a high degree of spatial and temporal variability due to different local sources, atmospheric stability and observation locations (e.g. Pataki et al. 2006).

Observations of $CO_2$ fluxes by eddy covariance ($F_{CO2,EC}$) systems in urban areas have been proven to be a reliable tool to assess carbon exchanges at the neighbourhood or local-scale when conducted above the roughness sublayer (RSL) (e.g. Grimmond et al. 2002; Nemitz et al. 2002; Feigenwinter et al. 2012). Urban areas are a net source of $CO_2$ (positive fluxes) due to emissions from road traffic, electricity production and local heating with natural gas, oil or coal. Daytime fluxes can be reduced by uptake from vegetation during the growing season, but the nocturnal respiration source remains (Kordowski and Kuttler 2010; Crawford et al. 2011; Ward et al. 2013). Where vegetation is scarce in cities, biogenic fluxes contribute little to the total net flux.

Diurnal concentrations of $CO_2$ vary within the boundary layer (BL) as a response to changes in surface emissions, boundary layer growth, entrainment processes and horizontal transport (advection). Taking into account the changing boundary layer (BL) volume and exchanges at its vertical and horizontal ‘boundaries’, meso-scale fluxes ($10^2$-$10^4$ km$^2$) can be inferred from diurnal changes in $CO_2$ concentrations observed in the BL, using the Integrative Mass Boundary Layer (IMBL) method (McNaughton and Spriggs 1986; Raupach et al. 1992; Denmead et al. 1996; Strong et al. 2011; Christen et al. 2014). The IMBL method has been applied over heterogeneous areas to calculate the mean regional $CO_2$ surface flux across, for example., the Amazonian basin (Lloyd et al. 2001, 2007) or an agricultural area in Spain (Font et al. 2010), while urban applications include nocturnal $CO_2$ and $CH_4$ emissions for Krakow (Poland) (Zimnoch et al. 2010) and turbulent sensible and latent heat fluxes in Sacramento (California, USA) (Cleugh and Grimmond 2001).

The aim of this study is to estimate top-down $CO_2$ emissions at the urban boundary layer (UBL) scale by the IMBL method using airborne observations taken in the UBL of Greater London (GL). This approach assumes that a representative urban $CO_2$ concentration can be calculated from a transect across a large area of the city or downwind of it. Results of the IMBL method are presented for four case study days, with a sensitivity analysis of the influence of different assumptions being made, and then compared to neighbourhood-scale eddy-covariance measurements and bottom-up emission inventory estimates. Conclusions from this study highlight the applicability of such airborne observations to quantify $CO_2$ exchanges of a large city and also highlight the methodological challenges encountered.

## 2 Methods

### 2.1 Instrumentation and survey design

The NERC-ARSF aircraft provided the BL observations between the 12 and 25 October 2011 over South-East England (Table 1). The plane instrumented with an AIMMS-20 Air Data Probe (Aventech Research Inc.) measured temperature, barometric pressure, three components of wind speed and horizontal wind direction, with an instrument accuracy of 0.05°C (temperature), 0.1 kPa (pressure), 0.5 $m \cdot s^{-1}$ (horizontal wind) and 0.75 $m \cdot s^{-1}$ (vertical wind) (Beswick et al. 2008). Atmospheric $CO_2$ dry mole fractions were measured with a non-dispersive infrared (NDIR) portable instrument, the $CO_2$ Airborne Analyzer System AOS Inc., at a frequency of 0.5 Hz with a mean precision and accuracy of ±0.23 ppm and ±0.28 ppm, respectively (Font et al. 2008 provide further details). $CO_2$ concentrations were traceable to the International Standards (WMO-X2007 scale). An isokinetic aerosol intake fed the GRIMM 1.129 Sky-optical particle counter that measured particle mixing ratio in the size range 0.25-32 µm at a frequency of 0.17 Hz.

Flights passed over GL at a height of ~360 m above ground level. The air security authority permitted two paths: SW to NE and SSE to NNW (Fig. 1). Flight path directions were chosen from these options to be best aligned with the prevailing wind direction on the respective day. Vertical profiles (up to 2200 m) were undertaken: just after take-off, before landing and on the perimeter of GL (Fig. 1).

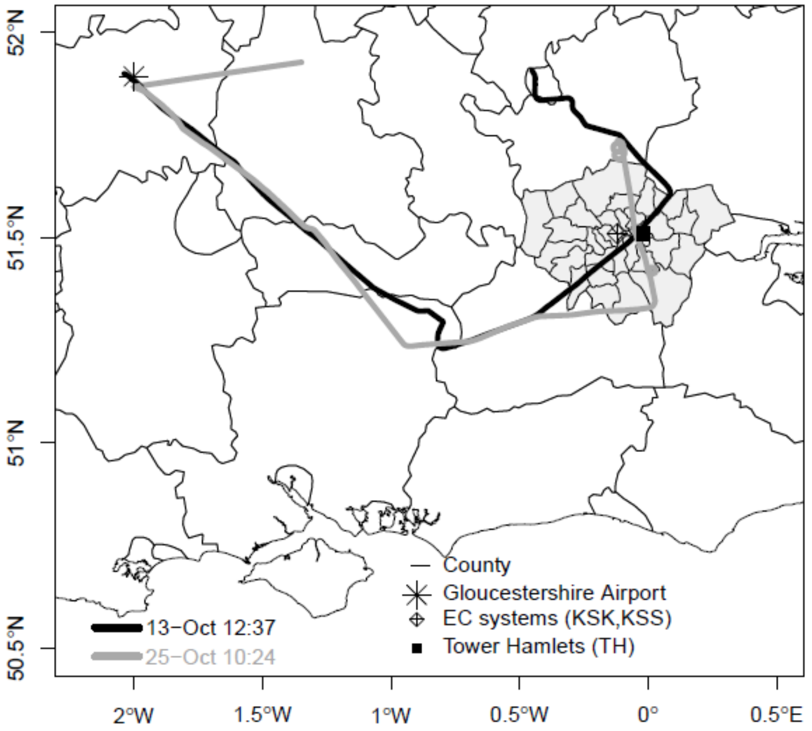

Figure 1. Flight tracks for 13 and 25 October 2011. GL is shaded and symbols indicate site locations of relevant surface stations.

UCL $CO_2$ mixing ratios were observed at Tower Hamlets (‘TH’; 51.51°N, 0.02°W, 9.2 m agl) (Fig. 1) every 15 minutes from the LiCOR-820 NDIR analyzer. Two-point calibrations are carried out every 15 days with a zero-scrubber (soda lime) and a $CO_2$ span gas referenced to the International Scale (WMO-X2007).

Neighbourhood-scale turbulent surface fluxes ($F_{CO2,EC}$) were measured at two long-term eddy covariance (EC) sites in central London (‘KSS’ and ‘KSK’; 51.51°N, 0.12°W). Measurement towers (KSS: Aluma T45-H triangular tower; KSK: single tube mast, Clark Masts CSQ T97/HP) had sensors at 49 m (KSS) and 39 m agl (KSK), about 2.2 x and 1.9 x mean building height in the flux source area, respectively. At both KSS and KSK, the EC system consisted of a CSAT3 sonic anemometer (Campbell Scientific) and a Li7500/Li7500A open path infrared gas analyser (LiCOR Biosciences). The data were sampled at 10 Hz and fluxes calculated for 30 minute intervals. Data processing and quality control are described in Kotthaus and Grimmond (2012, 2013a).

### 2.2 Surface fluxes from aircraft observations

The Integrative Mass Boundary Layer (IMBL) method, used to calculate spatially and temporally integrated urban $CO_2$ surface fluxes from the aircraft observations, treats the BL as a box with conserved scalars

(Denmead et al. 1996; Guenther et al. 1996). The variation of the mean mixed-layer $CO_2$ concentration (expressed in $\mu$mol$CO_2$ $m^{-3}$, $[CO_2]$) in time ($\partial[CO_2]/\partial t$) at the measurement height ($h$) within the BL, also known as storage flux ($F_{stg}$), is the result of the surface flux ($F_{CO2,\,IMBL}$), entrainment ($F_e$) and advection ($F_{adv}$):

$$h\frac{\partial[CO_2]}{\partial t} = F_{CO_2,IMBL} + F_e + F_{adv} \qquad (1)$$

$F_e$ is a function of the difference in concentration in the air entrained from above ($[CO_2]_+$), as the BL height ($h_L$) changes in time ($\partial h_L/\partial t$), under a vertical velocity ($w_+$), and within the BL ($[CO_2]$):

$$F_e = \left(\frac{\partial h_L}{\partial t} - w_+\right)([CO_2]_+ - [CO_2]) \qquad (2)$$

$F_{adv}$ is the product of the horizontal wind speed $U$ and the spatial $CO_2$ gradient ($\partial[CO_2]/\partial x$) at height h:

$$F_{adv} = -h\left(U\frac{\partial[CO_2]}{\partial x}\right) \qquad (3)$$

Reorganizing and integrating Eq. (1) in time, the surface flux can be calculated according to:

$$F_{CO_2,IMBL} = \langle h\rangle\frac{[CO_2]_2-[CO_2]_1}{t_2-t_1} - \left(\frac{h_{L2}-h_{L1}}{t_2-t_1} - w_+\right)([CO_2]_+ - \langle[CO_2]\rangle) + \langle h\rangle\langle U\rangle\left\langle\frac{\Delta[CO_2]}{\Delta x}\right\rangle \qquad (4)$$

where ‹› denotes temporal and spatial mean values, i.e. $\langle[CO_2]\rangle$ is the mean concentration over the whole spatial and temporal domain, $[CO_2]_2$ and $[CO_2]_1$ are the concentrations measured at times $t_1$ and $t_2$, respectively, with the respective mixing heights $h_{L1}$ and $h_{L2}$, and $w_+$ and $[CO_2]_+$ refer to $h_{L1}$ and $t_1$. $\langle\frac{\Delta[CO_2]}{\Delta x}\rangle$ is calculated via linear regression fit to $[CO_2]$ measured at time $t_1$ with distance when the plane track was perpendicular to the main wind direction.

$[CO_2]$ is calculated from $CO_2$ mixing ratios, temperature and barometric pressure measurements by the ideal gas law. Equation 4 is applied in two ways. The first approach assumes that the same temporal changes in emission rates occur at different locations so that the relative spatial distribution of $CO_2$ is constant in time. In this case temporal profiles of $[CO_2]$ measured during the horizontal transects are used. Vertical profiles of $CO_2$, particulates, temperature, wind speed and direction at take-off and landing were used to examine the depth of the BL and its changes in time. The second approach, the "column model" (Jacob, 1999), quantifies differences in $[CO_2]$ within vertical columns upwind and downwind of the city, both observed along vertical profiles. The composition of the well-mixed column varies while travelling across the surface due to emissions within the observational footprint.

### 2.3. Spatial representativeness of the measurements

To determine the likely source area of the BL observations used to calculate $F_{CO2,IMBL}$, the Lagrangian Particle Dispersion Model FLEXPART (Stohl et al. 2005) was used in backward mode. Using urban roughness values, FLEXPART is driven by the ECMWF meteorological model with 0.2° x 0.2°, 91 vertical levels and 3 h resolution. Ten thousand particles were released from a box defined by the aircraft track (longitude, latitude and altitude) for each transect or profile. Each simulation runs back to midnight at the start of the flight day. Analysis at 5 min intervals (0.05° x 0.05° spatial resolution) allows estimation of the mean residence time of the air in the layer 0 to 300 m agl that potentially influences the $CO_2$ concentrations.

The source area for the local-scale $F_{CO2,EC}$ is calculated for both flux towers for every 30 min period using the Kormann and Meixner (2001) footprint model. Sources located within a radius of about 1000 m around the KSS site contribute to the turbulent fluxes, with the closest 300 m responsible for 50% of the impact (Kotthaus and Grimmond, 2013b). The source area at KSK is a bit smaller, and individual roughness elements can impact the observations at times when the EC system is within the RSL. The source areas of both sites are dominated by road surfaces and buildings, with only very little contribution from vegetation. Kotthaus and Grimmond (2012) provide further details on micro-scale emissions within the EC source areas.

The source area for the concentration observations within the RSL are not formally calculated, but it is known that the integration area is larger for concentrations than flux measurements (Schmid, 1994) and within the RSL individual roughness elements and sources/sinks are more influential than at larger scales. It can be assumed that the local-scale $F_{CO2,EC}$ footprints are larger than the concentration source areas in the RSL and that flow channelling may elongate the latter along the streets.

### 2.4 Emissions inventory for Greater London

The Department of Energy and Climate Change reported annual $CO_2$ emissions by Local Authority (LA) for 2011 (DECC, 2014), segregated into four main categories: industrial and commercial; domestic; transport; and land use change and forestry. The uncertainty of the inventory for the LAs in GL ranges from 1.6 to 2.6% (MacCarthy, 2014).

To compare $F_{CO2,IMBL}$ with bottom-up fluxes ($F_{CO2,inv}$), the annual flux for GL in 2011 was scaled for the footprint area that influenced the airborne measurements as:

$$F_{CO2,inv} = \frac{E_{LA} * R_{t,LA}}{A_{GL} * \sum R_{t,LA}} \tag{5}$$

where $E_{LA}$ are annual emissions for each LA (kt$CO_2$ y$^{-1}$), $R_{t,LA}$ is the residence time of air masses in each LA based on the FLEXPART analysis, and $A_{GL}$ is the area of influence over London. Temporal profiles accounting for diurnal, day-of-week, and monthly variations of industrial and domestic emissions were calculated from energy demand statistics. Variations of transport emissions were calculated from temporal variations of roadside $NO_X$ increments in London. Further details on how temporal profiles were calculated are given in Appendix A.

## 3 Results

### 3.1 $CO_2$ mixing ratio observations

The spatial variability of $CO_2$ within and beyond the GL UBL during each flight is shown in Fig. 2. For lower wind speed conditions (<8 m s$^{-1}$ at 360 m), higher $CO_2$ mixing ratios were measured over central London, with peaks at 400.5 ppm (12 October 2011), 421.5 ppm (13 October) and 399.1 ppm (25 October), compared to ~394-398 ppm outside the GL area (Figure 2). With higher wind speed conditions (>8 m s$^{-1}$), the differences in average mixing ratio within and surrounding GL were within the instrument noise (e.g. 17, 24 October) (Table 1). However, for these conditions the maximum measured $CO_2$ mixing ratio in the mixing layer (407.2 and 409.5 ppm for 17 and 24 October, respectively) was registered downwind of GL at a distance of 29 km (17 October) and 48 km (24 October) from central GL (Fig. SB1).

Table 1. Mean wind speed (U), mean (±1 standard deviation σ), maximum and inter-quartile range (IQR) of $CO_2$ mixing ratios measured onboard the NERC-ARSF aircraft during the transects across GL (inGL) in October 2011 and surrounding GL (outGL) below 400 m.

| Date, time of flight (UT) | U inGL (m s$^{-1}$) | $CO_2$ ±1σ inGL (ppm) | Max $CO_2$ inGL (ppm) | IQR $CO_2$ inGL (ppm) | $CO_2$ ±1σ outGL (ppm) |
|---|---|---|---|---|---|
| 12 Oct 10:46 | 7.7 | 396.1 ± 1.6 | 400.5 | 1.9 | 392.8 ± 1.1 |
| 13 Oct 13:14 | 4.4 | 404.4 ± 3.3 | 411.4 | 1.2 | 397.5 ± 3.4 |
| 13 Oct 15:26 | 6.0 | 405.1 ± 7.5 | 421.8 | 12.6 | 398.2 ± 3.3 |
| 17 Oct 09:39 | 9.9 | 395.1 ± 2.8 | 399.2 | 5.1 | 394.9 ± 3.5 |
| 17 Oct 10:21 | 8.5 | 392.8 ± 1.4 | 396.1 | 2.3 | 393.5 ± 3.4 |
| 19 Oct 12:52 | 8.8 | 392.8 ± 0.9 | 395.9 | 0.9 | 392.3 ± 1.6 |
| 19 Oct 15:33 | 9.1 | 392.1 ± 0.9 | 396.6 | 1.1 | 391.3 ± 0.7 |
| 24 Oct 10:25 | 11.0 | 404.4 ± 1.6 | 407.9 | 2.7 | 404.4 ± 1.9 |
| 25 Oct 11:03 | 6.9 | 395.3 ± 1.7 | 399.1 | 2.6 | 394.3 ± 0.9 |
| 25 Oct 13:59 | 7.0 | 394.9 ± 1.0 | 397.0 | 1.3 | 393.7 ± 0.8 |

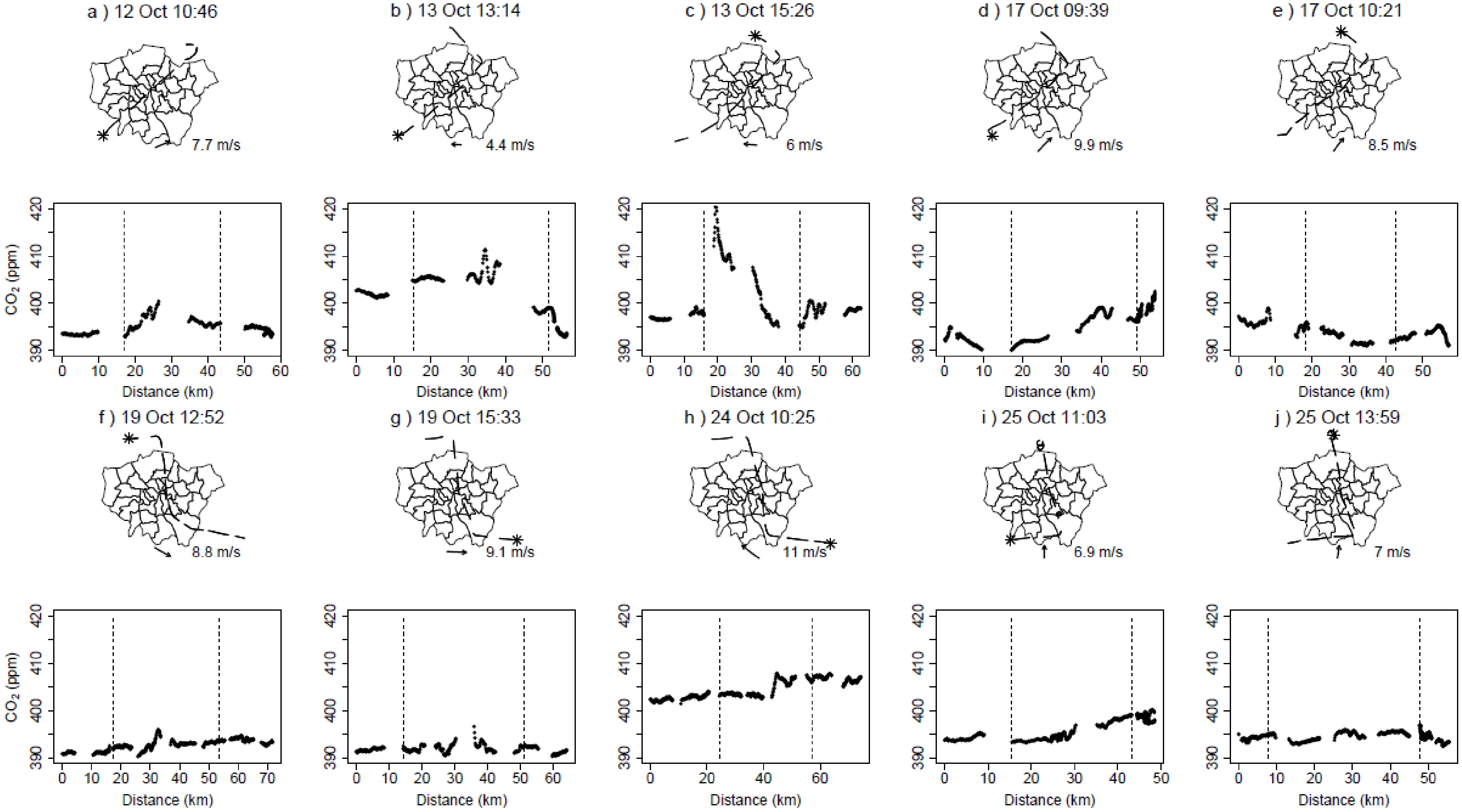

Figure 2. (Upper) Aircraft flight path over GL starting at location marked by *, with mean wind speed and direction (arrow) measured over GL. Time indicates the start of the transect over GL. (Lower) Measured $CO_2$ mixing ratios with distance from the indicated start point; vertical dashed lines indicate locations of GL boundary.

## 3.2 IMBL $CO_2$ fluxes in Greater London

Time and space integrated $F_{CO2,IMBL}$ for GL were calculated for 13, 17, 24 and 25 October when all terms of the IMBL budget could be identified and quantified. The two IMBL approaches outlined (Section 2.2) were each applied for two of the case study days. First, temporal variations of the mean [$CO_2$] measured along the transects over GL were used to calculate surface fluxes on 13 and 17 October. Second, downwind profiles were compared to upwind references on 24 and 25 October. Given sufficient data were not available, the IMBL method could not be applied to 12 October (only one transect measured), and 19 October (advection could not be quantified as the flight track was perpendicular to the main wind direction under high wind speeds, see Fig. 2).

### 3.2.1 $CO_2$ fluxes calculated from horizontal transects

The mean wind speed at 360 m over GL on 13 October was 4.4±1.1 m $s^{-1}$ (morning) and 6.0±1.2 m $s^{-1}$ (afternoon). Visual inspection of vertical profiles showed a well-mixed BL reaching up to a height of 735 m (morning) and at 1180 m (afternoon; Fig. SC1). The flight track flew over the TH site. Mixing ratios measured within the UCL were similar to those measured at 360 m: 405.6 ppm (TH) and 404.4 ppm (aircraft) at 13:15 UTC; 407.7 ppm (TH) and 405.1 ppm (aircraft) at 15:30 UTC, suggesting efficient mixing between the ground and flight altitude. The $F_{CO2,IMBL}$ estimate for this period (13:15 UTC to 15:30 UTC) was 50.7 µmol $CO_2$ $m^{-2}$ $s^{-1}$. According to the FLEXPART model, the probable source area of the airborne observations covered 71% of GL and included the east (residence time of air 60-80 s) and central boroughs (~20 s) (Fig. 3a,b).

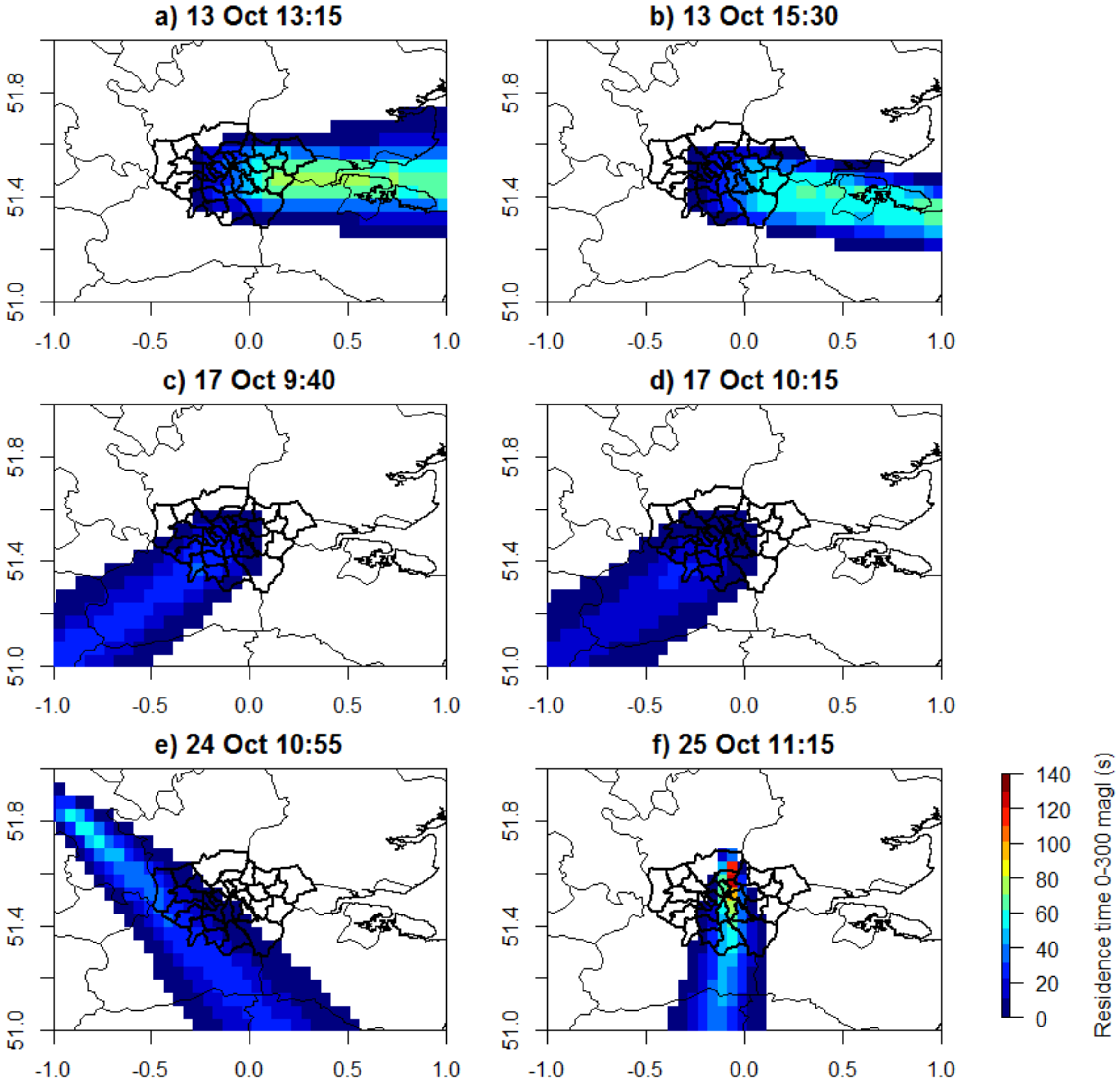

Figure 3. Air residence time in the layer 0-300 m above ground level (agl) estimated by FLEXPART for flights used in IMBL calculations (Table 2).

Table 2. Values used to calculate the space and time integrated $CO_2$ urban-regional scale flux ($F_{CO2,IMBL}$) in GL using the IMBL budget method. $F_{stg}$ is the storage flux, $F_e$ the entrainment flux and $F_{adv}$ the advection term. $F_{CO2\ inv}$, is the emissions estimated by DECC (2014).

| | 13 Oct | 17 Oct | 24 Oct | 25 Oct |
|---|---|---|---|---|
| $t_1$ (UTC) | 13:15 | 9:40 | 10:15 | 11:05 |
| $t_2$ (UTC) | 15:30 | 10:15 | 10:55 | 11:15 |
| $CO_2$ ($t_1$) (ppm) | 404.4 | 394.8 | 401.4 | 394.6 |
| $CO_2$ ($t_2$) (ppm) | 405.1 | 392.8 | 406.7 | 398.7 |
| $CO_{2+}$ (ppm) | 391.3 | 390.0 | 401.0 | 394.1 |
| $\langle CO_2 \rangle$ (ppm) | 404.7 | 393.7 | 401.4 | 394.6 |
| $h_1$ (m) | 735 | 400 | 410 | 450 |
| $h_2$ (m) | 1180 | 1130 | 480 | 450 |
| $w_+$ (mm $s^{-1}$) | -2.5 | -0.18 | -2.2 | -5.6 |
| $\langle U \rangle$ (m $s^{-1}$) | 4.5 | 9.9 | --- | --- |
| $\langle \frac{\Delta[CO_2]}{\Delta x} \rangle$ (µmol $CO_2$ $m^{-2}$) | --- | $1.1 \cdot 10^{-2}$ | --- | --- |
| $F_{stg}$ (µmol $CO_2$ $m^{-2}$ $s^{-1}$) | 0.3 | -21.5 | 25.7 | 103.3 |
| $F_e$ (µmol $CO_2$ $m^{-2}$ $s^{-1}$) | -50.4 | -29.5 | -11.6 | -1.1 |
| $F_{adv}$ (µmol $CO_2$ $m^{-2}$ $s^{-1}$) | --- | -37.9 | --- | --- |
| $F_{CO2,IMBL}$ (µmol $CO_2$ $m^{-2}$ $s^{-1}$) | 50.7 | 46.0 | 37.2 | 104.3 |
| $F_{CO2\ inv}$ (µmol $CO_2$ $m^{-2}s^{-1}$) | 42.7 | 54.5 | 60.4 | 145.1 |
| *Area GL covered (%)* | 71 | 56 | 50 | 30 |

Vertical profiles of temperature in the morning of 17 October indicated inversion layers at 390-436 m and at 460-500 m (Fig, SC2). This translated into a decrease in the $CO_2$ mixing ratios with altitude: ~401.5 (TH) and 395.1 ppm (aircraft). Later that day (11:56 UTC) the UBL attained 1130 m so that $CO_2$ mixing ratios were observed to be vertically homogenous below the cruise altitude (392.3 ppm at TH, 392.8 ppm at 360 m). Given the strong wind speed conditions and the flight track parallel to the main wind flow (Fig. 2), the 17 October was the only case study day when it was possible to calculate $\langle \frac{\Delta[CO_2]}{\Delta x} \rangle$ from Eq. 3 and $F_{adv}$ (Table 2). $F_e$ was negative as air masses with less concentration than below were entrained and $CO_2$ was lost by advection. $F_{stg}$ was negative due to the expansion of the UBL in time. At 46.0 µmol $CO_2$ $m^{-2}$ $s^{-1}$ $F_{CO2,IMBL}$ was in the same order of magnitude as on 13 October. The source area coincides with large parts of GL (65%), encompassing areas in central and south-west GL (Fig. 3c,d).

### 3.2.2 $CO_2$ fluxes calculated from upwind and downwind vertical profiles

On 24 and 25 October, strong wind speed conditions and the prevalent wind direction allowed Lagrangian observations of two vertical profiles, one upwind and the other downwind of GL. An increase of the $CO_2$ mixing ratio was observed in the downwind profiles compared to those upwind by 4-5 ppm (Fig. SC3, SC4).

Strong winds from the SE (12 m $s^{-1}$) were measured over GL at 360 m altitude on 24 October. Both the vertical profiles upwind and downwind of GL revealed large $CO_2$ mixing ratios of >400 ppm at low altitudes (<500 m), with a sharp decrease to lower values (391 ppm) above a capping inversion. The strong inversion conditions on that day might have resulted in a residual layer with large $CO_2$ mixing ratios. The height of the lowest inversion layer increased from 410 m (upwind) to 460 m (downwind). The derived flux $F_{CO2,IMBL}$ was similar in range to 13 and 17 October (37.2 µmol $CO_2$ $m^{-2}$ $s^{-1}$ between 10:10 and 10:57). The probable source area covered is 60% of GL with an emphasis of western parts (Fig. 3e).

On 25 October wind speeds were 7 m $s^{-1}$ with a prevailing flow from the south. Given no strong inversion was present, absolute mixing ratios were lower than on the preceding day and remained below 400 ppm. There was an increase of ~4 ppm from the upwind to the downwind locations but the very low entrainment flux as no changes in the UBL height were considered (Fig. SC4), translated to a very high $F_{CO2,IMBL}$ estimate of 104.3 µmol$CO_2$ $m^{-2}$ $s^{-1}$ between 11:05 and 11:15. The source area was estimated to be smaller than on the other case study days, covering only 30% of the GL including areas in north, central and south London (Fig. 3f).

### 3.2.3 Sensitivity analysis of $F_{CO2,IMBL}$

Sensitivity analyses allow quantification of the impact of values used within $F_{CO2,IMBL}$ calculations. Assuming uniform temporal changes, the spatial variability of [$CO_2$] at 360 m across GL relates to the differences in emissions at different locations (Table 1, Fig. 2). On one case study day (13 October), the standard deviation of [$CO_2$] measured along the transects were as high as 7.5 ppm and the inter-quartile range (IQR) reached up to 12.6 ppm. This spatial variation in mixing ratio suggests that there may have been a series of internal BL across GL and horizontal mixing did not have enough time to create a representative spatial pattern at the flight height (360 m). Standard deviation and IQR were generally lower for the other case studies (Table 1). As the [$CO_2$] values used to calculate $F_{CO2,IMBL}$ are critical, the variation of $CO_2$ along the transect was used to assess the accuracy of the flux calculated. Other variables that are used for the $F_{CO2,IMBL}$ calculations are: mixing layer height, vertical velocity at the top of the UBL and temporal and spatial homogeneity of the background concentration. The impact of potential uncertainties in these components on the total uncertainty of the integrated boundary layer $CO_2$ flux are assessed from the horizontal transects over the urban area and both upwind and downwind vertical profiles (Table 3).

Table 3. Sensitivity of $F_{CO2,IMBL}$ to data used in the analysis. *mean* $[CO_2]_a$: average mixing ratio from aircraft observations; *mean* $[CO_2]_{a+s}$ average mixing ratio from aircraft and urban canopy layer; $5^{th}p$ $[CO_2]_a$: $5^{th}$ percentile mixing ratio from aircraft observations; $95^{th}p$ $[CO_2]_a$ $95^{th}$ $95^{th}$ percentile mixing ratio from aircraft observations; *h+50m* and *h+100m* refer to mixing layer height determined from visual inspection from profiles carried outside GL plus 50 and 100 m, respectively; *no* $w_+$ and $2 \cdot w_+$ refer to zero and double vertical wind speed above the mixing layer, respectively; $F_{adv,t2}$ refers to advection term calculated using the spatial gradient at $t_2$. The median value and range (maximum-minimum) for the fluxes for each day are also given.

| | $F_{CO_2,IMBL}$ (μmolCO$_2$ m$^{-2}$ s$^{-1}$) | | | |
|---|---|---|---|---|
| *Method* | 13 Oct | 17 Oct | 24 Oct | 25 Oct |
| *mean* $[CO_2]_a$ | 50.7 | 46.0 | 37.2 | 104.3 |
| *mean* $\{[CO_2]_a + [CO_2]_s\}$ | 49.2 | 34.9 | --- | --- |
| $5^{th}$ *p* $[CO_2]_a$ | 30.7 | 41.6 | 34.5 | 133.8 |
| $95^{th}$ *p* $[CO_2]_a$ | 82.3 | 70.7 | 33.6 | 89.0 |
| *h + 50 m* | 56.1 | 48.0 | 42.8 | 136.8 |
| *h + 100 m* | 61.4 | 50.0 | 51.4 | 171.7 |
| *no* $w_+$ | 47.5 | 46.0 | 33.6 | 100.8 |
| $2 \cdot w_+$ | 54.0 | 46.0 | 45.2 | 146.3 |
| $F_{adv}$ $t_2$ | --- | 24.7 | --- | --- |
| *Median* $F_{CO_2}$ | 52.4 | 46.0 | 37.2 | 133.8 |
| *Range* $F_{CO_2}$ | 51.6 | 46.0 | 17.8 | 82.7 |

To evaluate the impact of horizontal spatial variability of [CO$_2$] on $F_{CO2,IMBL,}$ the mean values are replaced with the 5th and 95th percentile of [CO$_2$], respectively (Table 3). The resulting $F_{CO2,IMBL}$ varied from 30.7 to 82.3 μmolCO$_2$ m$^{-2}$ s$^{-1}$ (13 October) and from 41.6 to 73.0 μmolCO$_2$ m$^{-2}$ s$^{-1}$ (17 October). Use of these extreme [CO$_2$] values generates a difference of up to 60% in the flux relative to that calculated from the mean [CO$_2$].

Aircraft measurements at 360 m might not capture the vertical gradient within the whole UBL. CO$_2$ mixing ratios measured at TH were used to calculate $F_{CO2,IMBL}$. $F_{CO2,IMBL}$ decreased from 50.7 (aircraft) to 49.2 μmol CO$_2$ m$^{-2}$ s$^{-1}$ (aircraft+TH) (13 October), and from 46.0 (aircraft) to 34.9 μmol CO$_2$ m$^{-2}$ s$^{-1}$ (aircraft+TH) (17 October). Heterogeneity in the vertical domain in the UBL represent a change of 3% (13 October) and 25% (17 October) from $F_{CO2,IMBL}$ calculated from the mean [CO$_2$] in the transects.

Similarly, to evaluate the impact of the variability of the [CO$_2$] in the air column for fluxes calculated from upwind-downwind profiles, the 5th and 95th percentile values of [CO$_2$] were used. This resulted in an increase of $F_{CO2,IMBL}$ to 33.6 μmol CO$_2$ m$^{-2}$ s$^{-1}$ (using the 5th percentile) and to 34.5 μmol CO$_2$ m$^{-2}$ s$^{-1}$ (95th percentile) on 24 October (increase of ~56%). Whereas on 25 October, using the 5th percentile values of [$CO_2$] fluxes were 89.0 (decrease of 15%) but the 95th percentile resulted in a higher flux of 133.8 µmol $CO_2$ $m^{-2}$ $s^{-1}$ (increment of 28%). Unfortunately, UCL measurements of $CO_2$ directly below the vertical profiles were not available. However, the comparison of observations within the UCL with aircraft measurements near TH reveals that $CO_2$ mixing ratios hardly differed: 400 ppm (TH) and 400-402 (aircraft) on 24 October; 396 ppm (TH) and 395 ppm (aircraft) on 25 October. This indicates the $CO_2$ field below the aircraft was well-mixed, so little variation in $F_{CO2,IMBL}$ would be expected.

The advection term can be an important part of the $CO_2$ budget. Without transects parallel to the main wind direction (13 October) the spatial variability of $CO_2$ and therefore advection could not be quantified. Assuming that the spatial gradient measured on 17 October was the same as on 13 October, the estimated advection flux is 1.6 µmol $CO_2$ $m^{-2}$ $s^{-1}$ or a probable error in $F_{CO2,IMBL}$ of 4% from omitting advection for that day. However, for days with higher wind speeds (e.g. 17 October), omission of the advection term could represent an error of ~80%.

The uniformity in time of the spatial gradient might also be a source of uncertainty for the advection term. If the spatial gradient on 17 October was calculated at time $t_2$, the $F_{CO2,IMBL}$ would decrease by ~50% calculated to 24.7 µmol$CO_2$ $m^{-2}$ $s^{-1}$.

BL heights were estimated from profiles outside of London. Spanton and Williams (1988) found that the BL height in London could be 50-100 m higher than at a rural site. This in accordance with the difference found between the BL heights from the ceilometer at central London and from vertical profiles for the 24 October (day when backscattered data from ceilometer were clearly detected, Appendix C). $F_{CO2,IMBL}$ calculated with a BL 100 m higher resulted in larger fluxes by 21% (13 October), 5% (17 October), 38% (24 October) and 68% (25 October) compared to previous calculations. This test underlines the critical impact of the mixing height on $CO_2$ exchanges within the UBL.

As the small vertical velocity at the BL height is difficult to measure reliably from aircraft (Stull, 1988; Beswick et al. 2008), the sensitivity of $F_{CO2,IMBL}$ to errors in $w_+$ were examined assuming $w_+$=0 and doubling the observed $w_+$. Using the former ($w_+$ =0) $F_{CO2,IMBL}$ decreases by 6.4% (13 October), 0.1% (17 October), 10% (24 October), 3.3% (25 October). Whereas the latter (doubling) increases $F_{CO2,IMBL}$ by 6.4% (13 October), 21% (24 October) and 40% (25 October).

The entrainment flux is also be affected by the determination of $[CO_2]_+$. In this study we have used the concentration just above the mixing layer in vertical profiles undertaken outside GL, assuming that this concentration is spatially homogenous for the area between the city and the location of the vertical profile, and also for the integration time used in the IMBL calculations. Ideally, measurements of the entrainment concentration above the UBL would be used.

The range of $F_{CO2,IMBL}$ was lower (50-80% the median value) for fluxes calculated from upwind-downwind profiles compared to the range of fluxes from horizontal transects over the city (100%). However, this is as expected as single pairs of vertical profiles sample a limited area of the urban region (30-50%) compared to the area covered by horizontal transects (60-70%).

Our sensitivity analysis suggests that horizontal variability of the $CO_2$ field in the UBL, observed here by transects, is the most critical factor affecting $F_{CO2,IMBL}$. The determination of the BL height and vertical wind speed has more impact on $F_{CO2,IMBL}$ from upwind-downwind profiles.

### 3.2.4 $CO_2$ surface fluxes in Greater London

Aircraft-based $F_{CO2,IMBL}$ and tower-based $F_{CO2,EC}$ have complementary spatial and temporal resolutions and limitations (Lloyd et al. 2007; Desai et al. 2011). With two EC systems in central London, the intra-site variability in the $F_{CO2,EC}$ could be assessed (Fig 4a). The lower KSK site (smaller source area) is expected to be dominated by processes at the building-scale, while the taller KSS site is representative of the neighbourhood-scale (Kotthaus and Grimmond, 2013b) and $F_{CO2,IMBL}$ represent a larger area ($10^2$-$10^4$ km$^2$) and integrate processes at the city-scale.

Although direct comparison of $F_{CO2,EC}$ and $F_{CO2,IMBL}$ is not necessarily warranted given the lack of immediate correspondence, Levy et al. (1999) argue that results should be within the same range and show similar variation day-to-day. On 17 and 24 October, $F_{CO2,EC}$ and $F_{CO2,IMBL}$ have similar magnitude at the times when IMBL were calculated (Figure 4a), while the $F_{CO2,IMBL}$ is higher than the observed surface flux on 13 October and even more clearly so (by at least 20 µmol $CO_2$ m$^{-2}$ s$^{-1}$) on 25 October. These discrepancies may be explained partly by the uncertainties inherent in the IMBL method (Table 3), but the EC measurements may also underestimate the turbulent flux (as noted by Kotthaus and Grimmond 2013b). In terms of day-to-day variations, the EC and IMBL method both indicate similarly strong fluxes on 13, 17 and 24 October and also agree in estimating the largest fluxes on the 25 October.

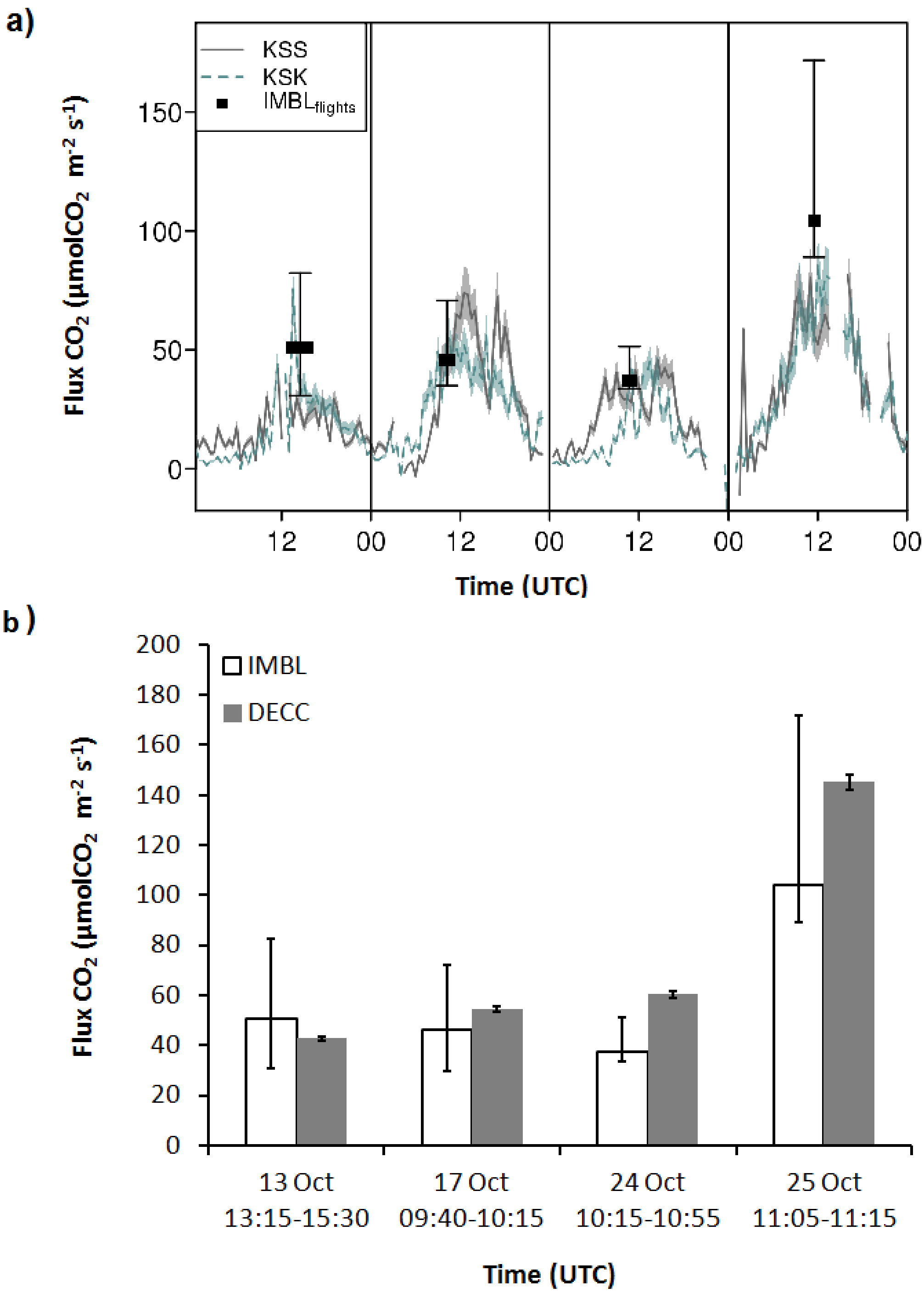

Figure 4 (a) Time series of turbulent fluxes of CO$_2$ as observed at eddy covariance sites KSS and KSK in central London (lines) and estimates from the aircraft observations (rectangles). The EC errors are shaded assuming ± 15% error on the 30 mins fluxes based on Euster et al. (1997), Dragoni et al. (2007) and Richardson et al. (2012) (b) Comparison of the surface fluxes calculated from aircraft observations (IMBL) against spatially integrated emissions as calculated from the DECC emissions inventory. Error bars on IMBL fluxes denote maximum and minimum values.

The annual $CO_2$ emissions for GL in 2011 were 18.3 μmol$CO_2$ $m^{-2}$ $s^{-1}$ (DECC, 2014). Scaling the footprint area for temporal variations of the emissions, IMBL fluxes are within -37% (24 October) and 19% (13 October) of the DECC emissions. The differences between the $F_{CO2,IMBL}$ and $F_{CO2,inv}$ on 24 October may relate to the $F_{CO2,IMBL}$ footprint area encompassing large areas outside GL (Fig. 3e) and/or the uncertainty in the temporal scaling.

Day-to-day differences in $F_{CO2,IMBL}$ are partly attributed to variations in the flux source area given that IMBL fluxes were calculated for similar times (except for 13 October). The DECC annual $F_{CO2,inv}$ has a concentric pattern: central GL boroughs have emissions of 50-350 μmol $CO_2$ $m^{-2}$ $s^{-1}$, surrounding centre boroughs 25-50 μmol $CO_2$ $m^{-2}$ $s^{-1}$, and outer boroughs <25 μmol $CO_2$ $m^{-2}$ $s^{-1}$. The highest $F_{CO2,IMBL}$ (October 25) was found when the footprint area encompassed the high emission central boroughs. Although the 17 October footprint also sampled central London, the calculated air residence times were shorter (10-30 s, Fig. 3c,d) (25 October, 70-140 s, Fig. 3f) and the probable footprint included the lower emission area of south-west GL. On 24 October the probable footprint extended over the outer boroughs to the west and south-west of GL (average annual emissions <25 μmol$CO_2$ $m^{-2}$ $s^{-1}$).

## 4 Discussion and conclusions

Here we have presented four airborne surveys that measured $CO_2$ mixing ratios in the UBL of GL in October 2011 that were used to estimate urban-scale emissions by quantifying boundary layer growth, entrainment processes and horizontal transport. The top-down inverse IMBL method infers temporally and spatially integrated fluxes that can be used to evaluate emissions inventories at policy-relevant scales such as cities, megacities, and oil and gas fields. Previously, this approach has been used to infer nocturnal fluxes of GHG with a single ground-level measurement site (Zimnoch et al. 2010), but inclusion of anthropogenic emissions for critical daytime activities was missing. Entrainment and advection fluxes are usually not considered in the calculations based on ground-level observations due to a lack of measurements at the top of the BL and the spatial gradient of $CO_2$. However, as shown in this study, the entrainment term (13 October) and advection (17 October) terms can be large fractions of the urban carbon budget. Observations from light aircraft characterize different parts of the budget to permit calculation of integrated regional surface $CO_2$ fluxes at larger scales than ground-level observations. Complementary aircraft surveys characterizing entrainment, vertical mixing and spatial heterogeneity in the UBL add value to continuous measurements at ground-level (Strong et al., 2011). However, aircraft observations are time-limited (e.g. plane time, flight path access) and weather-biased, so represent case studies.

The IMBL fluxes had similar day-to-day variability to both the central London eddy-covariance observations and the scaled (temporal, spatial) emissions inventory data. The IMBL fluxes are the same order as the eddy-covariance observations and within -37% to 19% of the emissions inventory. Thus the IMBL method appears to provide an additional independent estimate of city-scale fluxes to complement neighbourhood-scale eddy-covariance fluxes and emissions inventory data.

The sensitivity tests undertaken suggest differences of the order of 100% in $F_{CO2,IMBL}$ consistent with other city-scale fluxes derived from aircraft measurements using mass–balance approaches (e.g. for GHG Mays et al. 2009; Turnbull et al. 2011, $NO_X$ emissions Trainer et al. 1995). However, changes in UBL $CO_2$ concentration along large city transects may challenge city-wide emission quantification as this was the main source of uncertainty for IMBL fluxes. Atmospheric transport and surface exchange are continuous, creating a dynamic, complex picture in large cities that can hardly be resolved in short-term airborne campaigns (Gioli et al. 2014). This suggests that in a megacity such as London it may be necessary to consider internal boundary layers (IBL) within the city. The atmosphere above the outer boroughs, which are more extensive and typically have shorter roughness elements (e.g. buildings), may be well mixed, but over the central business district areas where the buildings are much taller the BL at the flight height may be the IBL for that area rather than the fully mixed UBL. Thus more detailed knowledge of the BL dynamics over urban areas is critical. Moreover, the rate of emission along a transect may temporally vary producing spatial variations of $CO_2$ within the UBL.

Downwind $[CO_2]$ enhancements above the background concentration are more representative of the mix of emissions taking place in the urban environment. A single pair of upwind-downwind profiles does not sample the entire urban area (Fig. 3e,f). In order to overcome this, multiple downwind profiles should be sampled in future surveys.

Footprint analysis allows identification of the areas potentially contributing to $CO_2$ concentrations in the UBL. Emissions from the inventory have been scaled for the footprint of airborne measurements and it might be a source of uncertainty. For better comparison of emissions and IMBL fluxes, meso-scale modelling such as the proposed by Brioude et al. (2013) could enhance better spatial scaling of the fluxes.

Anthropogenic and biogenic fluxes are inherently included in $F_{CO2,EC}$ and $F_{CO2,IMBL}$, whereas biogenic fluxes are missing from the $F_{CO2,\ inv}$ fluxes. The role of vegetation varies with amount (e.g. Helfter et al. 2011), but generally in urban areas it plays a small role in the $CO_2$ budget (Crawford et al. 2011, Strong et al. 2011;

Newman et al. 2013). In London the vegetation varies by size (age) and type across the city (Lindberg and Grimmond 2011). By October the role of vegetation is likely small during the daytime relative to urban sources even in suburban areas with a large amount of vegetation (Ward et al. 2013). To distinguish the anthropogenic signal, fast-response measurements of urban pollutants (e.g. $NO_X$, CO) as tracers of traffic-related emission and isotopic analysis of carbon (e.g. $^{13}C/^{12}C\text{-}CO_2$, $\Delta^{14}CO_2$) would aid interpretation. An emissions ratio approach (e.g. Turnbull et al. 2011) would allow apportionment and identification of the sectors emitting more $CO_2$ into the atmosphere and thus facilitate evaluation of policy effectiveness to reduce the contribution of GHG emissions from urban areas.

## Acknowledgements

The flights were undertaken as part of the ClearfLo project funded by the Natural Environment Research Council (NERC) and coordinated by the National Centre for Atmospheric Science (NCAS). The flights surveys were supported by the NERC-ARSF grant (GB11-05). We would like to thank the crew and the operations team of the ARSF team. We extend out thanks to Rebecca Fisher at Royal Holloway University of London (RHUL) for the calibration to the NOAA standards of the references used for the surface monitoring sites. We are grateful to the Lab of the Atmosphere and the Oceans from the Institut Català de Ciències del Clima (LAO-IC3) for the airborne $CO_2$ instrument and in-flight standards and the insightful comments of reviewers which improved the paper. The research was supported by the National Institute for Health Research (NIHR) Biomedical Research Centre based at Guy's and St Thomas' NHS Foundation Trust and King's College London and NERC ClearfLo (NE/H003231/1).

## Figures

Fig. 1: B&W (print version)

Fig. 2: B&W (print version)

Fig. 3: B&W (print version), Colour (web version)

Fig. 4: B&W (print and web version)

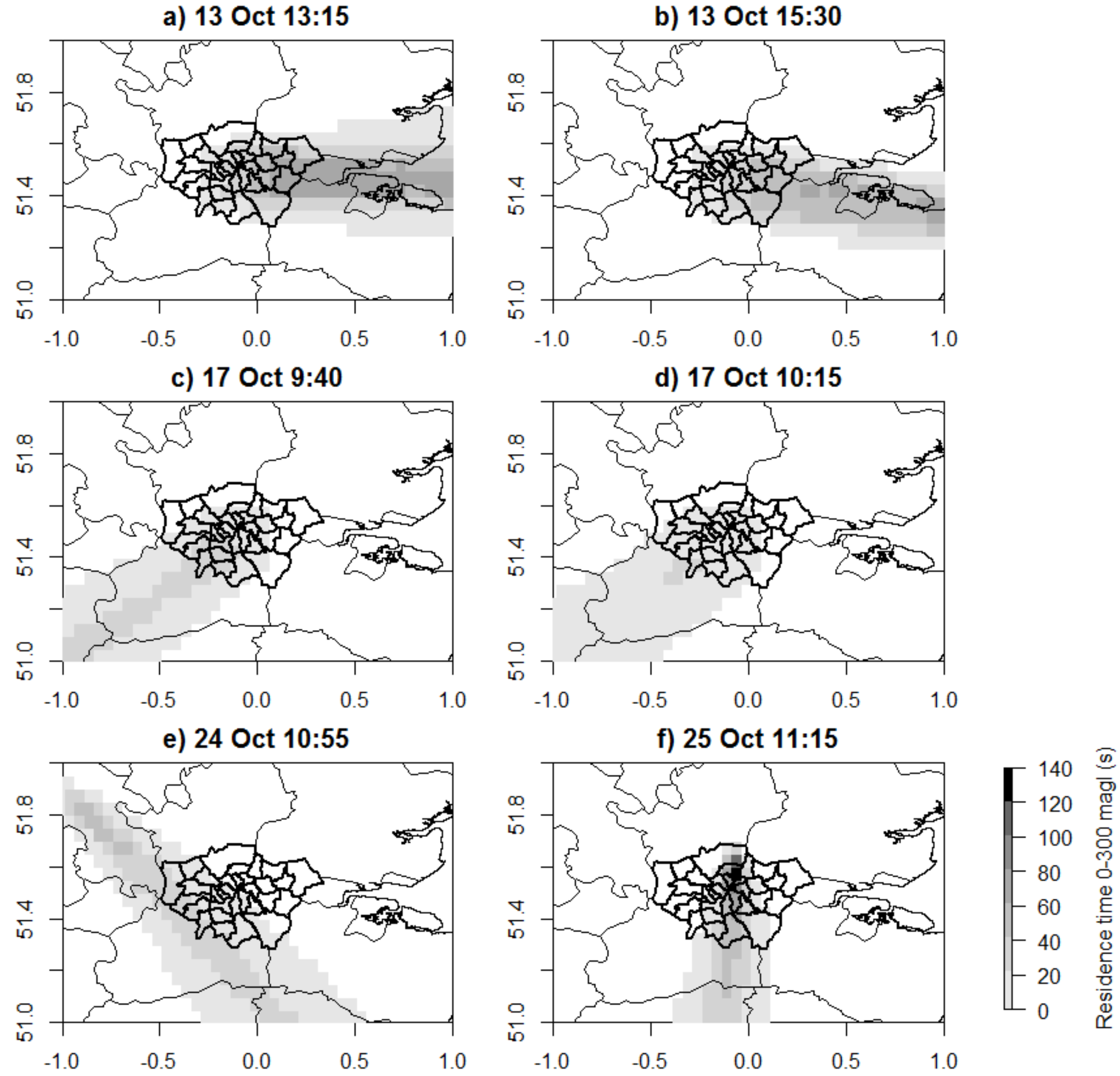

Figure 3 in B&W for print version

## References

Beswick, K.M., Gallagher, M.W., Webb, A.R., Norton, E.G. & Perry, F. (2008). Application of the Aventech AIMMS20AQ airborne probe for turbulence measurements during the Convective Storm Initiation Project. *Atmospheric Chemistry and Physics, 8*, 5449–5463.

Brioude, J., Angevine, W.M., Ahmadov, R., Kim, S.-W., Evan, S., McKeen, S.A., Hsie, E.-Y., Frost, G. J., Neuman, J.A., Pollack, I.B., Peischl, J., Ryerson, T.B., Holloway, J., Brown, S.S., Nowak, J.B., Roberts, J.M., Wofsy, S.C., Santoni, G.W., Oda, T., Trainer, M. (2013). Top-down estimate of surface flux in the Los Angeles Basin using a mesoscale inverse modeling technique: assessing anthropogenic emissions of

CO, NOx and $CO_2$ and their impacts, *Atmospheric Chemistry and Physics*, 13, 3661-3677, doi:10.5194/acp-13-3661-2013.

Christen, A. (2014). Progress in atmospheric measurement techniques to quantify greenhouse gas emissions from cities, *Urban Climate*, in press, doi: 10.1016/j.uclim.2014.04.006

Cleugh H.A., Grimmond, C.S.B. (2001). Modeling regional scale surface energy exchanges and CBL growth in a heterogeneous, urban-rural landscape. *Boundary Layer Meteorology, 98*, 1-31.

Crawford, B., Grimmond, C.S.B. & Christen, A. (2011). Five years of carbon dioxide fluxes measurements in a highly vegetated suburban area. *Atmospheric Environment, 45*, 1564–1573.

Denmead, O.T., Raupach, M.R., Dunin, F.X., Cleugh, H.A., Leuning, R. (1996). Boundary-Layer Budgets for Regional Estimates of Scalar Fluxes. *Global Change Biology, 2*, 255–264.

Department of Energy and Climate Change (DECC) (2014): https://www.gov.uk/government/statistics/local-authority-emissions-estimates (last access: 28 August 2014).

Desai, A.R., Moore, D.J.P., Ahue, W.K.M., Wilkes, P.T.V., De Wekker, S.F J., Brooks, B.G., Campos, T.L., Stephens, B.B., Monson, R.K., Burns, S.P., Quaife, T., Aulenbach, S.M., Schimel, D.S. (2011). Seasonal pattern of regional carbon balance in the central Rocky Mountains from surface and airborne measurements, *Journal Geophysical Research, 116*, G04009, doi:10.1029/2011JG001655.

Dragoni D., Schmid, H.P., Grimmond, C.S.B., Loescher, H.W. (2007) Uncertainty of annual net ecosystem productivity estimated using eddy covariance flux measurements, *Journal Geophysical* Research, 112, D17102.

Duren, R.M., Miller, C.E. (2012). Measuring the carbon emissions of megacities. *Nature Climate Change, 2*, 560-562.

Eugster, W., McFadden, J.P., Chapin, E.S. (1997). A comparative approach to regional variation in surface fluxes using mobile eddy correlation towers, *Boundary Layer Meteorology, 85*, 293–307.

Feigenwinter, C., Vogt, R., Christen, A. (2012). Eddy Covariance Measurements Over Urban Areas in Eddy Covariance, *Springer Atmospheric Sciences*, 377-397.

Font, A., Morguí, J.-A., Rodó, X. (2008). Atmospheric $CO_2$ in-situ measurements: two examples of Crown Design flights in NE Spain. *Journal of Geophysical Research, 113*, D12308, doi:10.1029/2007JD009111.

Font, A., Morguí, J.-A., Curcoll, R., Pouchet, I., Casals, I., Rodó, X. (2010). Daily carbon surface fluxes in the West Ebre (Ebro) watershed from aircraft profiling on late June 2007. *Tellus, 62B*, 427-440.

Gioli, B., Carfora, M. F., Magliulo, V., Metallo, M.C., Poli, A.A., Toscano, P., Miglietta, F. (2014). Aircraft mass budgeting to measure $CO_2$ emissions of Rome, Italy. *Environmental Monitoring and Assessment, 186*, 2053–2066, doi: 10.1007/s10661-013-3517-4.

Grimmond, C.S.B., King, T.S., Cropley, F.D., Nowak, D.J., Souch, C. (2002). Local-scale fluxes of carbon dioxide in urban environments: methodological challanges and results from Chicago. *Environmental Pollution, 116*, S243-S254.

Guenther, A., Zimmerman, P., Klinger, L., Greenberg, J., Ennis, C., Davis, K. & Pollock, W. (1996). Estimates of regional natural volatile organic compound fluxes from enclosure and ambient measurements. *Journal of Geophysical Research*, *101*, D1, 1345-1359.

Helfter, C., Famulari, D., Phillips, G. J., Barlow, J. F., Wood, C. R., Grimmond, C.S.B., Nemitz, E. (2011), Controls of carbon dioxide concentrations and fluxes above central London, *Atmospheric Chemistry and Physics, 11*, 1913–1928, doi:10.5194/acp-11-1913-2011.

International Energy Agency (IEA) (2008). World Energy Outlook, 2008, Paris, France

Idso, C.D., Idso, S.B. & Balling, R.C., Jr. (1998). The urban $CO_2$ dome of Phoenix, Arizona. *Physical Geography, 19*, 95-108.

Jacob, D.J. (1999). Introduction to Atmospheric Chemistry. *Princeton University Press*, 267 pp.

Kordowski, K., Kuttler, W. (2010). Carbon dioxide fluxes over an urban park area. *Atmospheric Environment*, 44, 2722-2730.

Kormann, R., Meixner, F. X. (2001). An Analytical Footprint Model for Non-Neutral Stratification. *Boundary Layer Meteorology, 99*, 207–224.

Kotthaus, S., Grimmond, C.S.B. (2012). Identification of Micro-scale Anthropogenic $CO_2$, Heat and Moisture Sources – Processing Eddy Covariance Fluxes for a Dense Urban Environment. *Atmospheric Environment, 57*, 301-316, doi: 10.1016/j.atmosenv.2012.04.024.

Kotthaus, S., Grimmond, C.S.B. (2013a). Energy exchange in a dense urban environment – Part I: temporal variability of long-term observations in central London, *Urban Climate*, in press.

Kotthaus, S., Grimmond, C.S.B. (2013b). Energy exchange in a dense urban environment – Part II: impact of spatial heterogeneity of the surface, *Urban Climate*, in press.

Levy, P.E., Grelle, A., Lindroth, A., Mölder, M., Jarvis, P.G., Kruijt, B., Moncrieff, J.B. (1999). Regional-scale $CO_2$ fluxes over central Sweden by a boundary layer budget method. *Agricultural and Forest Meteorology, 98–99*, 169–180.

Lindberg, F, Grimmond, C.S.B. (2011) Nature of vegetation and building morphology characteristics across a city: influence on shadow patterns and mean radiant temperatures in London, *Urban Ecosystems, 14*(4), 617-634, doi: 10.1007/s11252-011-0184-5

Lloyd, J., Francey, R J., Mollicone, D., Raupach, M.R., Sogachev, A., Arneth, A., Byers, J.N., Kelliher, F.M., Rebmann, C., Valentini, R., Wong, S.-C., Bauer, G., Schulze, E.-D. (2001). Vertical profiles, boundary layer budgets, and regional flux estimates for $CO_2$ and its $^{13}C/^{12}C$ ratio and for water vapor above a forest/bog mosaic in central Siberia. *Global Biogeochemical Cycles, 15(2),* 267–284, doi:10.1029/1999GB001211.

Lloyd, J., Kolle, O., Fritsch, H., De Freitas, S.R., Silva Dias, M.A.F., Artaxo, P., Nobre, A.D., De Araújo, A.C., Kruijt, B., Sogacheva, L., Fisch, G., Thielmann, A., Kuhn, U., Andreae, M.O. (2007). An airborne regional carbon balance for Central Amazonia. *Biogeosciences, 4*, 759-768.

MacCarthy (2014). Local and Regional Carbon Dioxide Emissions Estimates for 2005-2012 for the UK Technical Report, available at https://www.gov.uk/government/uploads/system/uploads/attachment_data/file/322833/20120624_Local_CO2_-_Technical_Report_2012.pdf (last access: 28August 2014).

Mays, K.L., Shepson, P.B., Stirm, B.H., Karion, A., Sweeney, C., Gurney K.R. (2009). Aircraft-Based Measurements of the Carbon Footprint of Indianapolis. *Environment Science Technology, 43,* 7816–7823.

McNaughton, K.G., Spriggs, T.W. (1986). A Mixed-Layer Model for Regional Evaporation. *Boundary-Layer Meteorology, 34*, 243–263.

Nemitz, E., Hargreaves, K.J., McDonald, A.G., Dorsey, J.R., Fowler, D. (2002). Micrometeorological measurements of the urban heat budget and $CO_2$ emissions on a city scale. *Environmental Science and Technology, 36(14)*, 3139-3146.

Newman, S., Jeong, S., Fischer, M. L., Xu, X., Haman, C. L., Lefer, B., Alvarez, S., Rappenglueck, B., Kort, E. A., Andrews, A. E., Peischl, J., Gurney, K. R., Miller, C. E., Yung, Y. L. (2013). Diurnal tracking of anthropogenic $CO_2$ emissions in the Los Angeles basin megacity during spring 2010, Atmos. Chem. Phys., 13, 4359-4372, doi:10.5194/acp-13-4359-2013.

Pataki, D.E., Bowling, D.R., Ehleringer, J.R., Zobitz, J.M. (2006). High resolution atmospheric monitoring of urban carbon dioxide sources. *Geophysical Research Letters, 33,* L03813, doi:10.1029/2005GL024822.

Raupach, M.R. (1992). Drag and Drag Partition on Rough Surfaces. *Boundary-Layer Meteorology, 60,* 375–395.

Richardson, A. D., Aubinet, M., Barr, A. G., Hollinger, D. Y., Ibrom, A., Lasslop, G., Reichstein, M. (2012). Uncertainty Quantification in M. Aubinet et al. (eds.), Eddy Covariance: A Practical Guide to Measurement and Data Analysis, Springer Atmospheric Sciences, Springer Science C Business Media B.V.

Schmid, H.P. (1994). Source Areas for Scalars and Scalar Fluxes. *Boundary Layer Meteorology, 67*, 293–318.

Spanton, A.M. & Williams, M.L. (1988). A comparison of the structure of the atmospheric boundary layers in central London and a rural suburban site using acoustic sounding. *Atmospheric Environment, 22 (2)*, 211–223.

Stohl, A., Forster, C., Frank, A., Seibert, P., Wotawa, G. (2005). Technical note: the Lagrangian particles dispersion model FLEXPART version 6.2. *Atmospheric Chemistry and Physics, 5*, 2461–2474.

Strong, C., Stwertka, C., Bowling, D.R., Stephens, B.B., Ehleringer, J.R. (2011), Urban carbon dioxide cycles within the Salt Lake Valley: A multiple-box model validated by observations, *Journal Geophysical Research., 116*, D15307, doi:10.1029/2011JD015693.

Stull, R. B. (1988). An Introduction to Boundary Layer Meteorology, Springer, New York.

Trainer, M., Ridley, B.A., Buhr, M.P , Kok, G., Walega, J., Hiibler, G., Parrish, D. D., Fehsenfeld, F. C. (1995), Regional ozone and urban plumes in the southeastern United States: Birmingham, a case study, *Journal Geophysical Research, 100*, D9, 18823-18834.

Turnbull, J.C., Karion, A., Fischer, M.L., Faloona, I., Guilderson T., Lehman, S J., Miller, B.R., Miller, J.B., Montzka, S., Sherwood T., Saripalli, S., Sweeney C. & Tans, P.P. (2011). Assessment of fossil fuel carbon dioxide and other anthropogenic trace gas emissions from airborne measurements over Sacramento, California in spring 2009. *Atmospheric Chemistry and Physics, 11*, 705–721, doi:10.5194/acp-11-705-2011.

Velasco, E., Roth, M. (2010). Cities as net sources of $CO_2$: review of atmospheric $CO_2$ exchange in urban environments measured by Eddy Covariance technique. *Geography Compass, 4*, 1238–1259, doi: 10.1111/j.1749-8198.2010.00384.x.

Ward, H. C., Evans, J.G., Grimmond, C.S.B. (2013). Multi-season eddy covariance observations of energy, water and carbon fluxes over a suburban area in Swindon, UK. *Atmospheric Chemistry and Physics, 13*, 4645–4666.

Zimnoch, M., Godlowska, J., Necki, J.M., Rozanski, K. (2010). Assessing surface fluxes of $CO_2$ and $CH_4$ in urban environment: a reconnaissance study in Krakow, Southern Poland. *TellusB, 62*, 573–580, doi: 10.1111/j.1600-0889.2010.00489.x.